Research Square

Preprints are preliminary reports that have not undergone peer review.
They should not be considered conclusive, used to inform clinical practice,
or referenced by the media as validated information.

A Reduced-Order Physics-Based Heat Transport Model for Spatiotemporal Heatwave Dynamics in Arid Environments: A UAE Case Study

Alireza Daneshkhah

alireza.daneshkhah@eau.ac.ae

Emirates Aviation University

Muner Abou Hasan

Emirates Aviation University

Yacob Tesfaldet

Emirates Aviation University

Hannah Al Ali

Emirates Aviation University

Aziz Khan

Prince Sultan University

Zindoga Mukandavire

Emirates Aviation University

Majdi Fanous

Coventry University

Research Article

Keywords: Heatwave dynamics, Heatwave persistence, Partial differential equations, Reduced-order modelling, Climate reanalysis, Arid environments

Posted Date: November 10th, 2026

DOI: https://doi.org/10.21203/rs.3.rs-11162621/v1

License: This work is licensed under a Creative Commons Attribution 4.0 International License.
Read Full License

Additional Declarations: No competing interests reported.

A Reduced-Order Physics-Based Heat Transport Model for Spatiotemporal Heatwave Dynamics in Arid Environments: A UAE Case Study

Alireza Daneshkhah[1*], Muner Abou Hasan[1], Yacob T. Tesfaldet[1], Hannah Al Ali[1], Aziz Khan[2], Zindoga Mukandavire[3], Majdi Fanous[4]

[1*]Faculty of Mathematics & Data Science, Emirates Aviation University, Dubai, United Arab Emirates.
[2]Department of Mathematics and Sciences, Prince Sultan University, Riyadh, Saudi Arabia.
[3]Institute of Research and Professional Training, Emirates Aviation University, Dubai, United Arab Emirates.
[4]Centre for Computational Science & Mathematical Modelling, Coventry University, Coventry, United Kingdom.

*Corresponding author(s). E-mail(s): alireza.daneshkhah@eau.ac.ae;
Contributing authors: eaus419@eau.ac.ae; yacob.tesfaldet@eau.ac.ae; hannah.alali@emirates.com; akhan@psu.edu.sa; zindoga.mukandavire@emirates.com; majdifanous@hotmail.com;

Abstract

Heatwaves are a major climate hazard in arid environments, affecting public health, infrastructure, energy demand, and environmental sustainability. This study develops a reduced-order, physics-based spatiotemporal framework for regional temperature reconstruction and heatwave analysis, using the United Arab Emirates as a case study. The framework is derived from an advection–diffusion heat-transport equation, while the implemented model adopts a reduced diffusion–forcing formulation driven by ERA5-derived surface solar radiation, sensible heat flux, and near-surface specific humidity. The model is solved on a structured grid using finite-difference discretisation and evaluated primarily through one-step reconstruction over a chronologically held-out test period. Heatwaves are identified using location-specific $\mathbf{90^{th}}$-percentile thresholds estimated

exclusively from training-period temperatures, together with a minimum duration of three consecutive days. The one-step reconstruction achieves an R^2 of 0.956, RMSE of 1.18°C, and MAE of 0.83°C; duration-based heatwave detection yields an F1-score of 0.843 and accuracy of 94.2%. A supplementary recursive experiment under prescribed ERA5 forcing and reference-based boundary conditions shows increasing error with integration horizon, with R^2 decreasing from 0.875 at 3 days to 0.761 at 30 days and RMSE increasing to 2.76°C. These results demonstrate that a parsimonious diffusion–forcing PDE can reproduce dominant regional temperature patterns and sustained heatwave behaviour while exposing the accumulation of structural error under recursive integration. The framework provides a reproducible baseline for future extensions involving explicit advection, irregular-domain discretisation, prognostic forcing, and hybrid physics–learning models.

Keywords: Heatwave dynamics, Heatwave persistence, Partial differential equations, Reduced-order modelling, Climate reanalysis, Arid environments

1 Introduction

Heatwaves are sustained periods of anomalously high temperature relative to local climatological conditions. Percentile-based thresholds combined with persistence criteria are widely used because they accommodate regional climatic differences and distinguish persistent events from isolated hot days (Perkins and Alexander, 2013; Robinson, 2001; Nairn and Fawcett, 2013). Extreme heat has important consequences for public health, labour productivity, infrastructure and energy systems (Kovats and Ebi, 2006; Gasparrini and Armstrong, 2011; Campbell et al., 2018; Arbuthnott and Hajat, 2017; Zuo et al., 2015), and its frequency, intensity and duration have increased in many regions under anthropogenic climate change (Guo et al., 2018; Lhotka et al., 2018; Liu et al., 2024). Arid and semi-arid regions are particularly exposed because strong radiative loading, sparse vegetation, dry land surfaces, coastal humidity gradients and rapid urbanisation interact to produce severe and persistent thermal stress. Urban expansion can further alter local heat storage and heatwave intensity through the urban heat-island effect (Lemonsu et al., 2015; Imran et al., 2019).

The United Arab Emirates (UAE) provides a relevant testbed for regional heatwave modelling. Its relatively compact domain combines extensive desert, major coastal cities, two coastlines and eastern mountainous terrain, producing substantial spatial variability in near-surface temperature. Regional climate projections for the Middle East and North Africa indicate further increases in maximum temperature and persistent heatwaves under future warming (Varela et al., 2020). Physically interpretable methods that can reproduce regional temperature evolution and persistent extreme heat are therefore useful for climate-risk assessment and as a foundation for subsequent adaptation-oriented modelling and climate services (Brimicombe et al., 2021; Vanderplanken et al., 2021).

Existing heatwave studies span empirical indices, statistical trend analysis, health-risk mapping and surveillance, data-driven prediction, and comprehensive atmospheric

modelling (Michelozzi et al., 2010; Buscail et al., 2012; Perkins, 2015). Statistical and machine-learning approaches can provide strong predictive performance but may offer limited direct interpretation of heat-transport mechanisms (LeCun et al., 2015; Reichstein et al., 2019; Karpatne et al., 2017). Conversely, numerical weather-prediction and regional climate models resolve substantially more atmospheric physics but require greater computational resources, complex boundary conditions and extensive parameterisation (Powers et al., 2017; Skamarock et al., 2019). This leaves a useful intermediate modelling scale for reduced-order, physics-based frameworks that retain a transparent connection between measurable environmental forcing and temperature evolution.

This study asks whether the dominant spatiotemporal evolution of daily near-surface temperature and persistent heatwave behaviour can be represented by a parsimonious heat-transport model driven by meteorological forcing. We derive a general advection–diffusion formulation and implement a reduced diffusion–forcing PDE in which environmental forcing is constructed from ERA5-derived surface solar radiation, sensible heat flux and near-surface specific humidity. The model is calibrated chronologically, solved on a structured grid, and evaluated using a held-out test period. The primary experiment is a conditional one-step reconstruction that assesses the local behaviour of the heat-transport operator under prescribed initial and boundary conditions; a recursive multi-step experiment quantifies structural error accumulation when the interior state is propagated for up to 30 days.

The principal contributions are: (i) a physically interpretable reduced-order formulation linking regional temperature tendency to diffusive redistribution and measurable environmental forcing; (ii) a transparent finite-difference implementation using processed ERA5-derived data at 48 fixed spatial locations; (iii) a leakage-controlled evaluation using chronological training, validation and held-out test subsets, training-only heatwave thresholds, pointwise and spatial diagnostics, and forcing-only comparison; and (iv) a recursive multi-step assessment that clarifies the capability and limitations of the reduced formulation beyond daily reinitialisation. The objective is not to replace operational forecasting systems, but to establish a reproducible intermediate-scale model that can be extended to explicit advection, heterogeneous transport coefficients, irregular domains and physics-informed learning.

2 Physics-Based Heat-Transport Model

2.1 Governing formulation

Let $T(\mathbf{x}, t)$ denote near-surface air temperature over a horizontal domain $\Omega \subset \mathbb{R}^2$, where $\mathbf{x} = (x, y)$. A reduced local conservation statement for thermal energy is

$$\frac{\partial T}{\partial t} = -\nabla \cdot \mathbf{J} + Q(\mathbf{x}, t), \tag{1}$$

where $\mathbf{J}$ is the horizontal heat-flux vector and Q is an effective environmental forcing expressed as a temperature tendency. Decomposing $\mathbf{J} = \mathbf{J}_{\text{diff}} + \mathbf{J}_{\text{adv}}$, with

$$\mathbf{J}_{\text{diff}} = -\alpha(\mathbf{x}, t)\nabla T, \qquad \mathbf{J}_{\text{adv}} = \mathbf{v}(\mathbf{x}, t)T, \tag{2}$$

and assuming locally incompressible horizontal flow gives

$$\frac{\partial T}{\partial t} = \nabla \cdot (\alpha \nabla T) - \mathbf{v} \cdot \nabla T + Q(\mathbf{x}, t). \tag{3}$$

Here α is an effective turbulent diffusivity and $\mathbf{v}$ is horizontal wind velocity. The diffusion term represents unresolved turbulent redistribution of thermal energy over the spatial scale of the model rather than molecular heat conduction. The advection term represents directional transport by the resolved horizontal circulation, while Q represents the aggregate temperature-tendency contribution of the environmental forcing. Equation (3) is therefore a reduced convection–diffusion representation rather than a complete atmospheric model; unresolved vertical structure, turbulent closure, land-surface exchange and mesoscale circulation are represented only indirectly.

The general formulation is useful because it separates three physically distinct mechanisms—local temperature tendency, spatial redistribution and directional transport—while remaining computationally tractable. In the present study, however, the objective is narrower: to determine how much of the daily regional temperature evolution can be reconstructed from diffusion plus measurable forcing before introducing additional transport complexity. The present implementation therefore deliberately omits explicit horizontal advection in order to isolate the contributions of diffusive redistribution and measurable environmental forcing. The implemented PDE is therefore

$$\frac{\partial T}{\partial t} = \nabla \cdot (\alpha \nabla T) + Q(\mathbf{x}, t). \tag{4}$$

For the daily implementation, Q has units of temperature tendency. The omission of advection is a modelling simplification, not an assumption that advective transport is physically unimportant; its consequences are evaluated through residual and recursive analyses and discussed in Section 6.

2.2 Environmental forcing and physical interpretation

The environmental forcing is represented conceptually as

$$Q(\mathbf{x}, t) = \tilde{\beta}_1 R_s(\mathbf{x}, t) + \tilde{\beta}_2 H(\mathbf{x}, t) - \tilde{\beta}_3 q(\mathbf{x}, t), \tag{5}$$

where R_s denotes incoming surface solar radiation, H denotes sensible heat flux under an upward-positive convention, and q denotes near-surface specific humidity. The coefficients $\tilde{\beta}_i$ are effective scaling parameters rather than fundamental physical constants. Surface solar radiation provides the radiative heating predictor; H represents land-to-atmosphere sensible heat exchange under the adopted upward-positive convention; and specific humidity is used as a moisture-related predictor rather than as an explicit

latent-heat-flux term. Because the three predictors have different units and are mutually correlated, the operational implementation standardises them before fitting and interprets the resulting coefficients as effective temperature-tendency weights. The forcing is therefore a calibrated reduced-order representation of the net influence of these predictors on daily temperature tendency, not a closed surface-energy balance. Unresolved effects such as land-cover heterogeneity, urban processes, soil-moisture feedbacks and coastal circulations remain potential sources of residual structure.

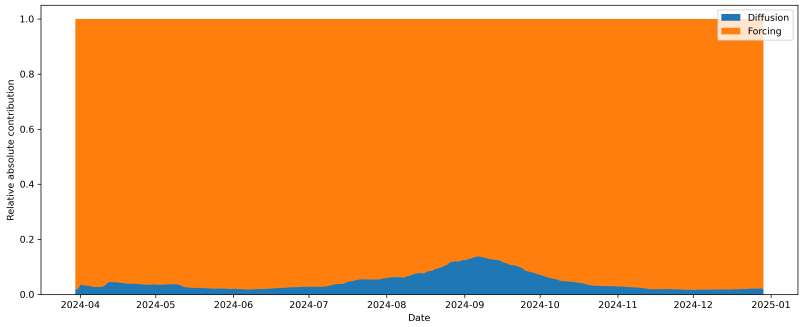


Fig. 1 Relative absolute contributions of the diffusion and forcing terms to the reduced-order PDE during the held-out reconstruction period.

Figure 1 shows that the calibrated forcing dominates the daily temperature tendency, while diffusion contributes a smaller but seasonally varying share. This finding motivates the explicit forcing-only comparison in Section 5.1 and cautions against interpreting the diffusion parameter as strongly identified from one-step reconstruction alone.

2.3 Heatwave definition

Let $T_{\mathrm{ref},j}(t)$ denote the daily reference temperature at evaluation location j. The location-specific heatwave threshold is estimated exclusively from the training period:

$$T_{90,j} = Q_{0.90}\left[T_{\mathrm{ref},j}(t) : t \in \mathcal{T}_{\mathrm{train}}\right], \tag{6}$$

where $Q_{0.90}$ denotes the empirical 90^{th} percentile. For either the reference or reconstructed series $T_j(t)$, an instantaneous exceedance is

$$E_j(t) = \mathbb{I}[T_j(t) > T_{90,j}]\,. \tag{7}$$

A duration-based heatwave indicator marks every day belonging to an exceedance run lasting at least $d_{\min} = 3$ consecutive days:

$$W_j(t) = \mathbb{I}[\exists\, a, b :\ a \le t \le b,\ b - a + 1 \ge d_{\min},\ E_j(s) = 1\ \forall s \in \{a, \ldots, b\}]\,. \tag{8}$$

The same fixed threshold $T_{90,j}$ is applied to the reference and reconstructed series. This prevents test-period leakage and ensures that classification differences arise from reconstruction error rather than from different threshold definitions.

3 Numerical Framework

3.1 Grid, spatial discretisation and time integration

The processed dataset contains daily values at 48 fixed spatial locations. These point-wise variables are interpolated onto an 80×60 regular grid before the PDE is solved. On this grid, the diffusion operator is approximated using the standard five-point central-difference Laplacian,

$$\nabla_h^2 T_{i,j} = \frac{T_{i+1,j} - 2T_{i,j} + T_{i-1,j}}{\Delta x^2} + \frac{T_{i,j+1} - 2T_{i,j} + T_{i,j-1}}{\Delta y^2}. \tag{9}$$

The reduced model is advanced using explicit forward Euler integration,

$$T_{i,j}^{n+1} = T_{i,j}^n + \Delta t \left[\alpha \nabla_h^2 T_{i,j}^n + F_{i,j}^n\right], \tag{10}$$

where F is the implemented forcing field defined in Section 4.2. For constant α, a sufficient two-dimensional diffusion-stability condition is

$$\alpha \Delta t \left(\frac{1}{\Delta x^2} + \frac{1}{\Delta y^2}\right) \leq \frac{1}{2}. \tag{11}$$

The scheme is first-order accurate in time and second-order accurate for diffusion. Explicit advection is not discretised in the present implementation because it is not included in Eq. (4).

3.2 Parameter estimation and effective diffusivity

The implemented model contains an effective diffusivity α and forcing coefficients. For each candidate α, the forcing coefficients were estimated from the training data using constrained ridge-regularised least squares. The three forcing predictors were standardised before calibration. For a generic predictor Z,

$$Z^* = \frac{Z - \mu_Z}{\sigma_Z}, \tag{12}$$

where μ_Z and σ_Z are estimated from the data used for forcing calibration. For a prescribed α, the regression target is the reference daily temperature tendency after subtracting the discrete diffusion contribution,

$$y = \frac{T_{\mathrm{ref}}^{n+1} - T_{\mathrm{ref}}^n}{\Delta t} - \alpha \nabla_h^2 T_{\mathrm{ref}}^n. \tag{13}$$

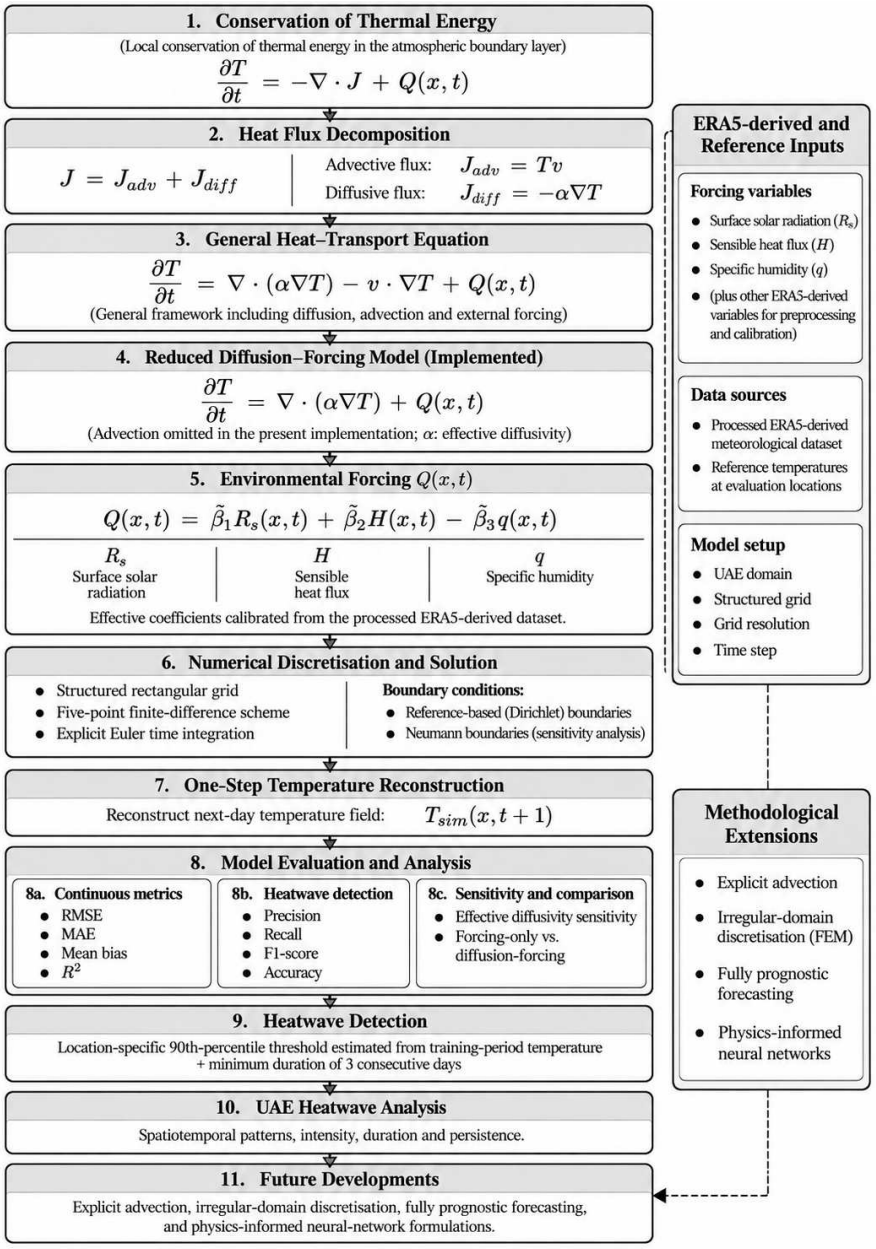


Fig. 2 Schematic overview of the reduced-order heatwave-modelling framework, linking the conservation equation to environmental forcing, numerical solution, one-step reconstruction, heatwave evaluation and future methodological extensions.

The coefficient vector is then obtained from

$$\min_{\boldsymbol{\beta}} \ \|\mathbf{y} - \mathbf{X}\boldsymbol{\beta}\|_2^2 + \lambda\|\boldsymbol{\beta}\|_2^2, \qquad \beta_1, \beta_2, \beta_3 \geq 0, \tag{14}$$

with an unpenalised, unconstrained intercept. The ridge term stabilises estimation in the presence of correlation among the ERA5-derived predictors, while the non-negativity constraints preserve the intended sign structure of the conceptual forcing model.

The candidate α producing the minimum validation-period one-step RMSE was selected, after which the forcing coefficients were refitted using the combined training and validation data before final held-out evaluation. The selected value was $\alpha = 2\ \mathrm{km^2\,day^{-1}}$, but the validation RMSE was almost invariant over $0 \leq \alpha \leq 2\ \mathrm{km^2\,day^{-1}}$. Accordingly, α is treated as a numerically selected effective parameter rather than a uniquely identified physical estimate. The final fitted coefficients were $c_0 \approx 0.00181\ ^\circ\mathrm{C\,day^{-1}}$, $\beta_1 = 0.1293$, $\beta_2 \approx 0$, and $\beta_3 = 0.0332$ for the standardised solar-radiation, upward sensible-heat-flux and specific-humidity predictors, respectively. The near-zero β_2 should not be interpreted as evidence that sensible heat exchange is physically unimportant because the predictors are correlated and each coefficient represents an incremental contribution conditional on the others.

3.3 Reconstruction and evaluation design

The primary experiment is a conditional one-step reconstruction. For each daily interval, the reference temperature field at time t initialises the interior state, the environmental forcing is prescribed, and the model advances one day to produce $T_{\mathrm{sim}}(\mathbf{x}, t + \Delta t)$. This design evaluates the local dynamical behaviour of the reduced PDE without allowing long-term integration error to dominate. It therefore measures reconstruction fidelity rather than autonomous forecasting skill. This distinction is important because high one-step agreement may arise partly from the accurate prescribed initial state; the forcing-only comparison and recursive experiment are therefore included explicitly to quantify what the diffusion operator contributes beyond that conditioning.

A supplementary recursive experiment evaluates 1-, 3-, 5-, 7-, 10-, 15- and 30-day horizons. For each reconstruction origin, the reference field is used only at the beginning of the integration window; subsequent interior states are generated recursively. ERA5-derived forcing and reference-based Dirichlet boundary values remain prescribed throughout the window. The recursive experiment is therefore a controlled multi-step reconstruction, not a free-running forecast.

Continuous performance is summarised using RMSE, MAE, mean bias and R^2. Heatwave classification is evaluated using accuracy, precision, recall and F1-score for both instantaneous threshold exceedance and the duration-based definition in Eq. (8). Residuals are defined consistently as

$$\epsilon(\mathbf{x}, t) = T_{\mathrm{ref}}(\mathbf{x}, t) - T_{\mathrm{sim}}(\mathbf{x}, t). \tag{15}$$

4 UAE Case Study and Implementation

4.1 Study region, data and spatial interpolation

The analysis covers January 2020 to December 2024. The processed dataset contains ERA5-derived atmospheric and land-surface variables at 48 fixed spatial locations across the UAE, including 2 m air temperature, solar radiation, sensible and latent heat fluxes, dew-point temperature, surface pressure, land-surface thermal variables and wind components. ERA5 is produced by ECMWF through assimilation of observations within a numerical weather-prediction system; in this study, however, the numerical solver does not consume native ERA5 grid cells directly. Instead, it uses the processed daily point dataset described below. The present workflow uses the available daily values directly; no additional sub-daily aggregation is performed, and one reference temperature value is available per evaluation location and day. Accordingly, the exact upstream daily statistic is not redefined by the PDE workflow and the heatwave thresholds are calculated from the daily values as supplied in the processed dataset.

The computational domain is formed from the minimum and maximum input coordinates with 2% padding, giving approximately

$$51.84^\circ\mathrm{E} \le \lambda \le 56.42^\circ\mathrm{E}, \qquad 22.62^\circ\mathrm{N} \le \phi \le 25.68^\circ\mathrm{N}, \tag{16}$$

and is discretised on an 80×60 grid with mean spacings $\Delta x \approx 5.88$ km and $\Delta y \approx 5.72$ km.

For each day and required variable, point values are mapped to the grid using inverse-distance weighting (IDW) based on the eight nearest input locations:

$$\widehat{Z}(\mathbf{x}, t) = \frac{\sum_{m \in \mathcal{N}_8(\mathbf{x})} w_m(\mathbf{x}) Z(\mathbf{x}_m, t)}{\sum_{m \in \mathcal{N}_8(\mathbf{x})} w_m(\mathbf{x})}, \qquad w_m(\mathbf{x}) = \frac{1}{d_m(\mathbf{x})^2}. \tag{17}$$

The same procedure is applied independently to the daily reference temperature and to each forcing variable. The eight-neighbour, inverse-square weighting gives larger influence to nearby input locations while providing a spatially continuous field on the structured grid required by the finite-difference solver. Thus, the numerical model does not operate directly on the native ERA5 grid; it operates on gridded fields constructed from the processed 48-location dataset. The interpolated reference field is also the source of the initial and boundary values used in the conditional reconstruction experiments, so spatial-field comparisons are not interpreted as independent validation against an external gridded product.

Dates were divided chronologically into 70% training, 15% validation and 15% held-out test subsets: 1 January 2020–1 July 2023, 1 July 2023–30 March 2024, and 30 March–30 December 2024, respectively. Adjacent subsets share one boundary date only to initialise the first transition. Heatwave thresholds were estimated exclusively from the training-period reference series and then fixed for validation and test evaluation.

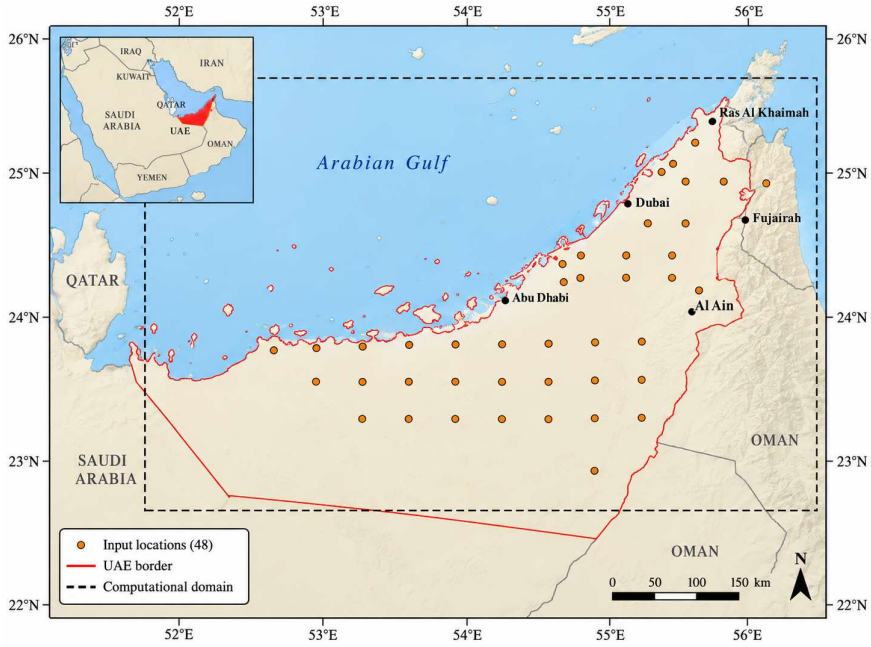


Fig. 3 Spatial distribution of the 48 fixed input locations used in the UAE case study and the rectangular computational domain employed by the reduced-order PDE model. The input locations are plotted using their exact longitude–latitude coordinates from the processed dataset. The dashed rectangle denotes the computational domain spanning approximately 51.84°E–56.42°E and 22.62°N–25.68°N. Selected major locations are labelled for geographical reference. Country boundaries and coastlines are based on Natural Earth geographic data.

4.2 Forcing implementation

For numerical calibration, the conceptual forcing in Eq. (5) is implemented using standardised predictors:

$$F(\mathbf{x},t) = c_0 + \beta_1 R_s^*(\mathbf{x},t) + \beta_2 H^*(\mathbf{x},t) - \beta_3 q^*(\mathbf{x},t), \tag{18}$$

where $Z^* = (Z - \mu_Z)/\sigma_Z$ and the standardisation parameters are estimated from the data used for forcing calibration. Sensible heat flux is expressed using an upward-positive convention,

$$H(\mathbf{x},t) = -H_{\mathrm{ERA5}}(\mathbf{x},t). \tag{19}$$

When direct specific humidity is unavailable, q is derived from the available dew-point temperature and surface pressure. The sign adjustment in Eq. (19) is applied before standardisation so that the physical and numerical definitions of H are consistent. For numerical robustness, the fitted forcing tendency is clipped to $[-5, 5]$ $^\circ\mathrm{C\,day}^{-1}$ before integration. Only R_s, H and q enter Eq. (18) as independent forcing predictors; the remaining variables in Table 1 support preprocessing, reference construction or physical interpretation.

Table 1 ERA5-derived variables used in the reduced diffusion–forcing implementation.

Meteorological variable	ERA5 identifier	Role in the model
2 m air temperature	t2m	Model initialisation and reference evaluation
Surface solar radiation	SSRD	Direct radiative predictor R_s
Sensible heat flux	SSHF	Direct predictor H; sign-adjusted to upward-positive
Latent heat flux	SLHF	Supporting interpretation; not a direct forcing predictor
Surface pressure	SP	Used in derivation of specific humidity
2 m dew-point temperature / specific humidity	d2m/q	Moisture-related predictor q
Skin temperature	SKT	Supporting land-surface interpretation

4.3 Initial and boundary conditions and computational workflow

For each one-step reconstruction interval, the interpolated reference field provides the initial condition,

$$T(\mathbf{x}, t_n) = T_{\mathrm{ref}}(\mathbf{x}, t_n), \tag{20}$$

and reference temperatures are prescribed on the outer boundary,

$$T(\mathbf{x}, t) = T_{\mathrm{ref}}(\mathbf{x}, t), \qquad \mathbf{x} \in \partial\Omega. \tag{21}$$

These values are taken from the interpolated reference-temperature field rather than from independent boundary observations. Prescribing the outer boundary reduces artificial edge effects while allowing the interior to evolve according to the reduced PDE. The same reference-based boundary treatment is retained in the recursive experiment. Consequently, the primary experiment is a conditional one-step reconstruction and all reported multi-step results are conditioned on known forcing and prescribed boundary values. Neither experiment should be interpreted as an independent external validation or as a fully prognostic forecast.

Spatial comparisons use the interpolated reference field and are therefore held-out reconstruction assessments rather than independent validation against an external gridded product. Pointwise comparisons at representative locations, including Abu Dhabi, Dubai, Al Ain and Fujairah, likewise use reference temperatures from the processed dataset. This distinction is maintained throughout the results.

5 Results

5.1 One-step reconstruction and incremental contribution of diffusion

Figure 5 compares reference and one-step reconstructed temperatures at representative evaluation locations during the held-out test period. The reconstructed trajectories

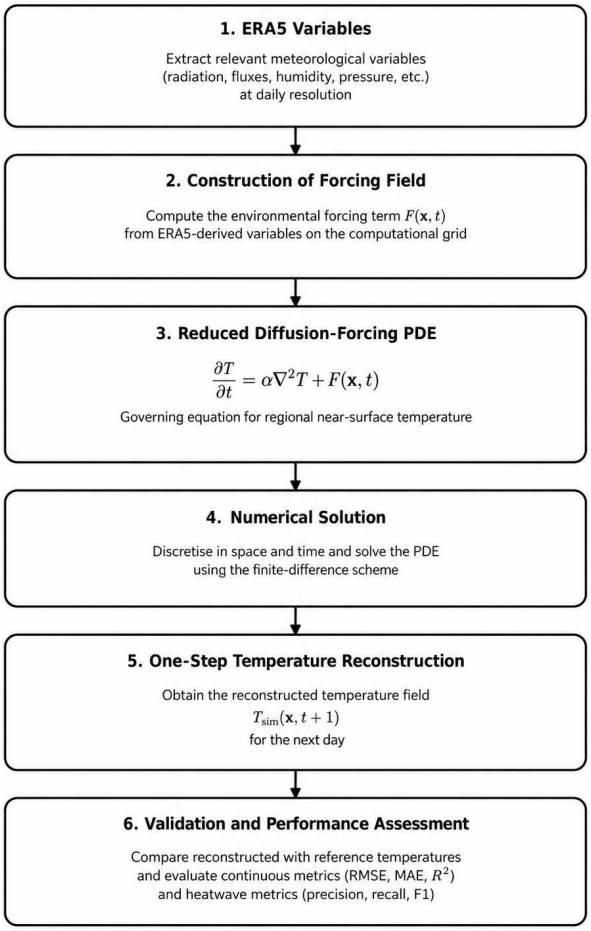


Fig. 4 Computational workflow for the UAE implementation, from ERA5-derived variables and gridded forcing to finite-difference solution, one-step reconstruction and performance assessment.

reproduce the dominant seasonal cycle and much of the day-to-day variability. Aggregate one-step performance is RMSE = 1.18°C, MAE = 0.83°C, $R^2 = 0.956$, and mean bias = −0.014°C. The near-zero aggregate bias does not imply uniform performance across temperature regimes; the pointwise and residual analyses below show larger dispersion under some extreme and transitional conditions.

Validation RMSE varies only from approximately 1.2307°C to 1.2306°C across $0 \leq \alpha \leq 2$ km^2 day^{-1}, confirming weak identifiability of the effective diffusivity at the adopted daily resolution. Figure 6 illustrates this flat sensitivity.

The incremental role of diffusion was assessed against a forcing-only formulation fitted under the same calibration procedure. Table 2 shows almost identical one-step performance, demonstrating that most daily reconstruction accuracy arises from the

Algorithm 1 One-step implementation of the reduced diffusion–forcing model

Require: ERA5-derived environmental variables, reference temperature fields $T_{\mathrm{ref}}(\mathbf{x}, t)$, effective diffusivity α, and time step Δt

Ensure: Reconstructed temperature fields $T_{\mathrm{sim}}(\mathbf{x}, t + \Delta t)$

for each daily reconstruction interval t **do**
    Extract the required meteorological variables at time t
    Interpolate the required pointwise variables onto the computational grid
    Construct $F(\mathbf{x}, t)$ using Eq. (18)
    Initialise $T(\mathbf{x}, t) \leftarrow T_{\mathrm{ref}}(\mathbf{x}, t)$
    Advance Eq. (4) by one finite-difference time step
    Compute $T_{\mathrm{sim}}(\mathbf{x}, t + \Delta t)$
    Evaluate $\epsilon \leftarrow T_{\mathrm{ref}} - T_{\mathrm{sim}}$
    Store the reconstructed field and residual
end for

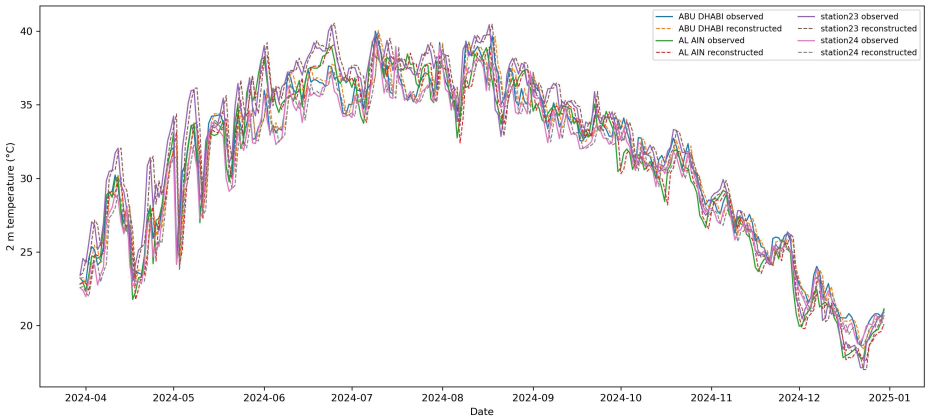


Fig. 5 Reference and one-step reconstructed near-surface temperatures at selected UAE evaluation locations over the held-out test period from March to December 2024.

prescribed initial state and environmental forcing, while diffusion provides only a marginal one-day improvement.

Table 2 Forcing-only and reduced diffusion–forcing one-step reconstruction over the held-out test period.

Model	RMSE (°C)	MAE (°C)	R^2
Forcing-only formulation	1.181	0.834	0.9559
Reduced diffusion–forcing formulation	1.180	0.833	0.9559

The daily tendency calibration itself is much weaker ($R^2 = 0.010$, RMSE $= 1.279$°C day^{-1}, MAE $= 0.920$°C day^{-1}). This is not inconsistent with the one-step reconstruction result: tendency regression must explain the full day-to-day increment from

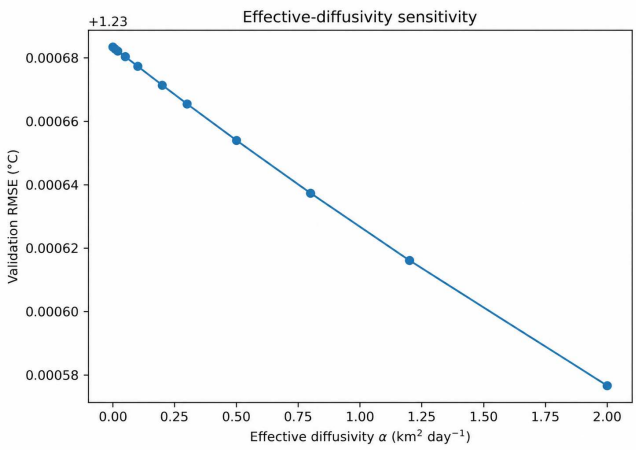


Fig. 6 Validation RMSE across the investigated range of effective diffusivity α.

forcing and diffusion, whereas one-step temperature reconstruction is initialised from the reference state at each interval.

5.2 Spatial and residual structure

Representative spatial fields are shown in Fig. 7. Across spring, summer, autumn and winter dates, the reconstruction preserves the dominant regional gradients and seasonal evolution represented by the interpolated reference fields. Reconstructed fields are generally smoother, particularly where local gradients are sharp, which is consistent with the uniform effective diffusivity and reduced-order formulation.

Residual maps provide a complementary view of geographically structured error. In early spring, coherent positive and negative residual regions are evident and most errors remain within approximately ± 2°C. Under peak-summer conditions, the residual field is substantially smoother and the majority of errors are within approximately ± 1°C. Autumn again shows stronger organised structure, especially over parts of the inland domain, while winter residuals are comparatively small and homogeneous. These patterns indicate that error is not purely random and that transitional regimes are more difficult for the reduced model than persistent summer and winter conditions.

The structured residuals are consistent with several unresolved mechanisms, including spatially varying transport, coastal circulations, land-surface heterogeneity and urban effects. Because these processes are not separately identified by the present experiment, the residual patterns cannot be attributed uniquely to omitted advection. They instead identify regimes in which the reduced diffusion–forcing representation is least complete.

5.3 Pointwise and residual-distribution evaluation

Figure 12 shows a strong pointwise relationship between reference and reconstructed temperature across the held-out evaluation locations. Most points lie close to the 1:1

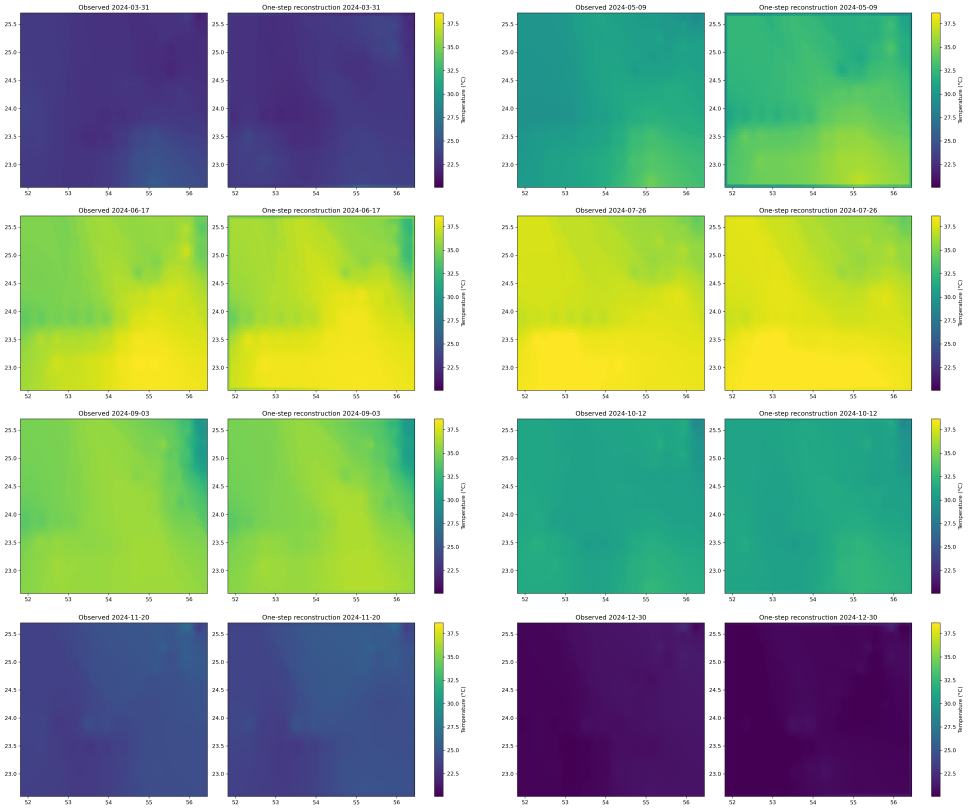


Fig. 7 Reference and one-step reconstructed near-surface temperature fields at representative dates from March to December 2024.

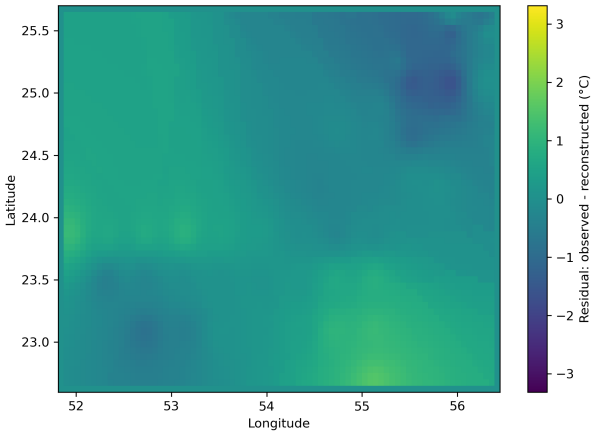


Fig. 8 Spatial residual field during early spring conditions (31 March 2024).

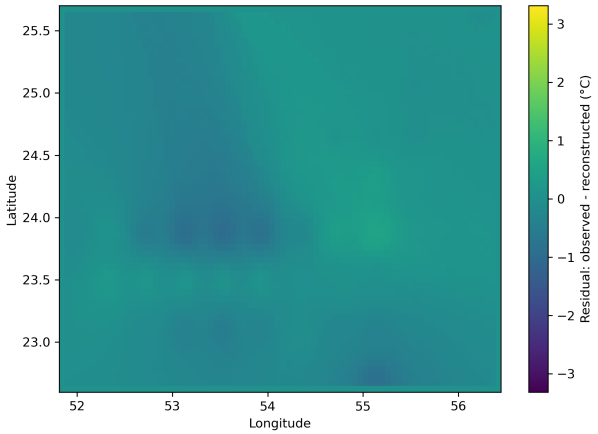


Fig. 9 Spatial residual field under peak-summer conditions (26 July 2024).

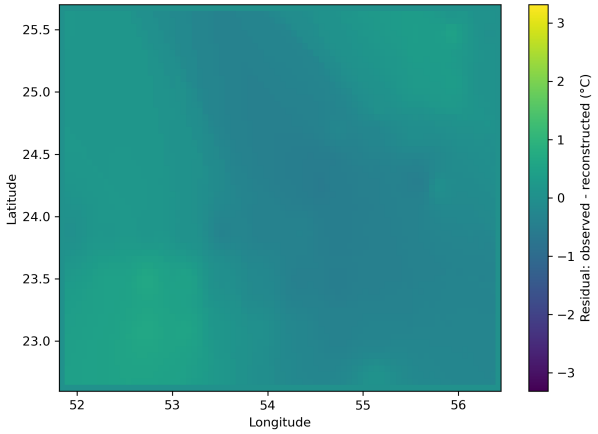


Fig. 10 Spatial residual field during autumn transition (12 October 2024).

line over the approximate 12–41°C range, consistent with the aggregate R^2 value. Dispersion increases at the upper end of the temperature range, and a small number of outliers occurs at intermediate temperatures. At high temperatures, reconstructed values also show a weak tendency to fall below the reference values. This temperature-dependent behaviour is important for heatwave classification because relatively small errors near a location-specific threshold can change the exceedance label even when overall continuous-error metrics remain strong.

The aggregate residual distribution in Fig. 13 is centred close to zero but exhibits non-Gaussian tails. Occasional larger positive or negative errors therefore coexist with negligible mean bias. The distribution should be interpreted together with the spatial and temperature-dependent diagnostics rather than as evidence of uniformly constant error variance.

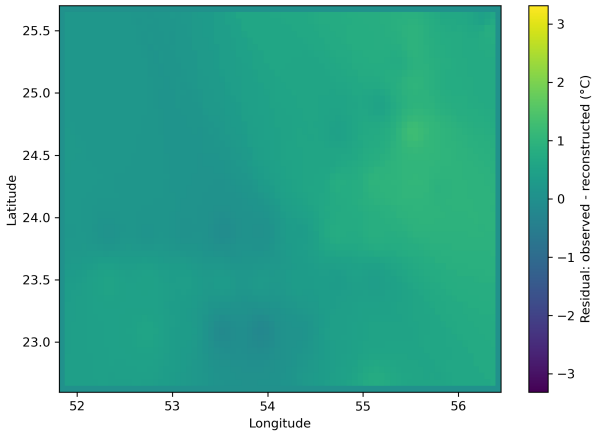


Fig. 11 Spatial residual field under winter conditions (30 December 2024).

5.4 Heatwave detection

Using the fixed training-derived 90^{th}-percentile thresholds without a persistence criterion, instantaneous exceedance classification over the held-out test period yields accuracy = 91.5%, precision = 0.778, recall = 0.811, and F1 = 0.794. Because non-exceedance days are more common, accuracy is interpreted jointly with precision and recall. Requiring at least three consecutive exceedance days improves the duration-based metrics to accuracy = 94.2%, precision = 0.822, recall = 0.866, and F1 = 0.843. The improvement indicates that sustained extreme-temperature conditions are reconstructed more reliably than isolated threshold crossings and that temporal persistence reduces sensitivity to small one-day errors around the threshold.

Figure 14 shows that the reconstructed fraction of evaluation locations in a duration-based heatwave generally follows the timing and clustering of the reference series. Differences in peak spatial extent remain, consistent with smoothing and threshold sensitivity near local extremes.

5.5 Recursive multi-step reconstruction

The recursive experiment removes daily reinitialisation of the interior state while retaining prescribed ERA5-derived forcing and reference-based boundary values. Table 3 shows that reconstruction error generally increases with horizon, although the trajectory is not strictly monotonic because different horizons sample different origin–target combinations and meteorological regimes.

At 3 days, $R^2 = 0.875$ and RMSE = 1.974°C; at 10 days, $R^2 = 0.829$ and RMSE = 2.309°C; and at 30 days, $R^2 = 0.761$ and RMSE = 2.755°C. Bias becomes progressively more negative, reaching −1.103°C at 30 days, which corresponds to an increasing warm bias because bias is defined as $T_{\text{ref}} - T_{\text{sim}}$. Heatwave F1 decreases from 0.843 at one day to 0.620 at 30 days; at 30 days recall remains high (0.878) while precision falls to 0.479, consistent with the warm bias generating additional threshold exceedances.

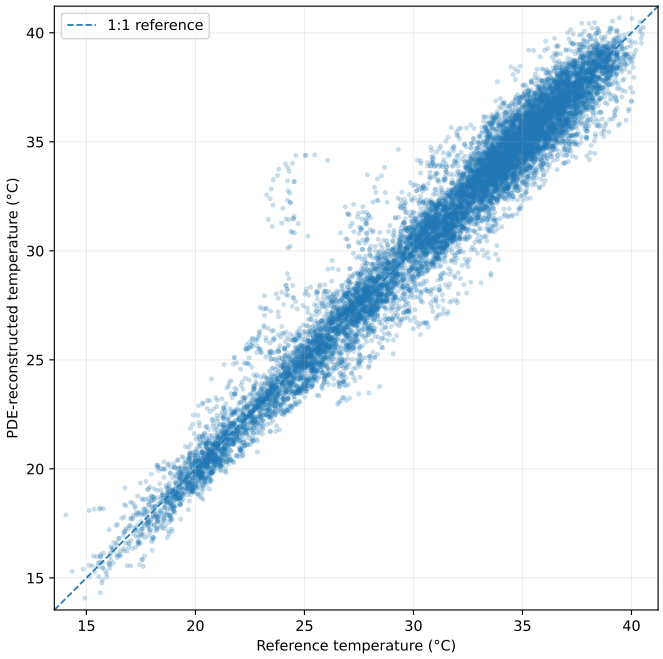


Fig. 12 Pointwise comparison between reference and PDE-reconstructed temperatures across representative evaluation locations and held-out test-period time points. The dashed line denotes the 1:1 reference.

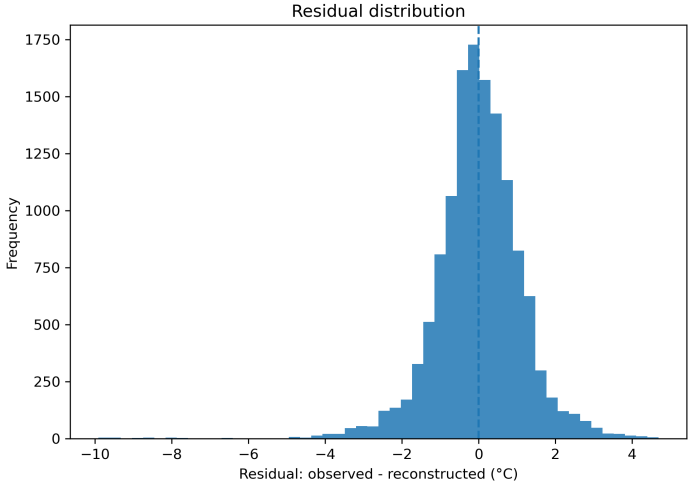


Fig. 13 Distribution of reconstruction residuals (reference minus PDE-reconstructed temperature) across evaluation locations and held-out test-period time points.

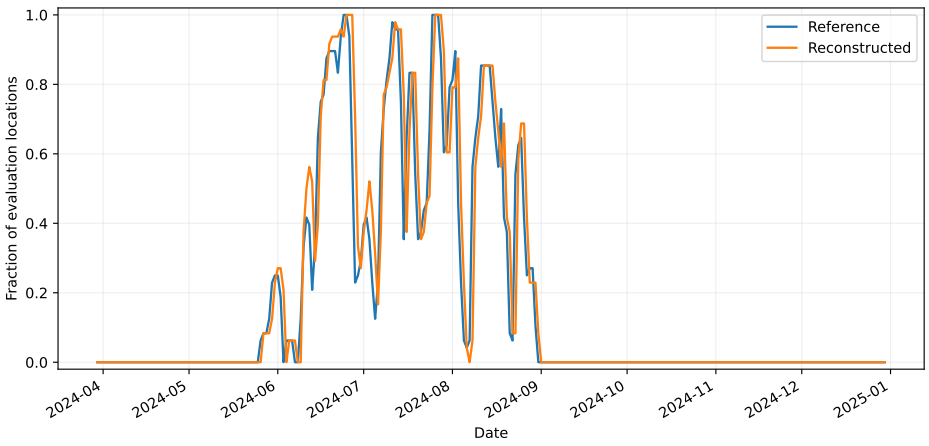


Fig. 14 Temporal evolution of reference and one-step reconstructed duration-based heatwave occurrence over the held-out test period, expressed as the fraction of evaluation locations satisfying the location-specific training-period 90^{th}-percentile threshold for at least three consecutive days.

Table 3 Recursive multi-step reconstruction over the held-out test period. Bias is reference minus reconstructed temperature; heatwave F1 uses the duration-based definition.

Horizon (days)	RMSE (°C)	MAE (°C)	Bias (°C)	R^2	Heatwave F1
1	1.182	0.836	-0.014	0.956	0.843
3	1.974	1.470	-0.048	0.875	0.670
5	2.172	1.632	-0.102	0.849	0.644
7	2.155	1.693	-0.162	0.851	0.637
10	2.309	1.799	-0.288	0.829	0.606
15	2.084	1.656	-0.541	0.863	0.644
30	2.755	2.236	-1.103	0.761	0.620

A companion forcing-only recursive comparison shows that the diffusion–forcing model has lower RMSE at every evaluated horizon. The relative reduction in RMSE increases from approximately 0.06% at one day to 0.55% at 3 days, 0.98% at 5 days, 1.41% at 7 days, 1.85% at 10 days, 2.77% at 15 days and 4.27% at 30 days; the corresponding R^2 advantage also increases with horizon. Thus, environmental forcing dominates the short-term reconstruction, whereas the incremental effect of diffusion becomes progressively more evident when the temperature field is propagated recursively. These results should still be interpreted as controlled reconstruction under prescribed forcing and boundaries, not as long-range operational forecasting performance.

6 Discussion

The results support three main conclusions about the reduced-order formulation and clarify how its strong reconstruction scores should be interpreted. First, conditional one-step reconstruction is accurate at the daily scale, but the forcing-only comparison

shows that this accuracy is dominated by the prescribed initial temperature field and calibrated environmental forcing. The diffusion term produces only a small one-day improvement and its selected coefficient is weakly identifiable under the current temporal and spatial resolution. This finding is important because it prevents over-attribution of one-step performance to the PDE diffusion operator.

Second, the recursive experiment exposes structural behaviour that is largely hidden by daily reinitialisation. Error grows with horizon and a systematic warm bias develops, while the incremental advantage of diffusion over the forcing-only model becomes larger. The reduced model therefore retains useful large-scale structure over multi-day integration but accumulates errors that limit its interpretation as a prognostic atmospheric model. Prescribed future forcing and reference-based boundaries further distinguish this experiment from operational forecasting.

Third, residual and threshold analyses identify where the simplifications matter. Errors become more dispersed at high temperatures and exhibit coherent spatial patterns during some transitional periods. These features are consistent with the possibility that omitted directional transport, spatially varying turbulent exchange, coastal processes, land-surface heterogeneity and urban effects contribute to the remaining discrepancy. The present analysis does not identify these mechanisms separately, so the error structure should not be attributed uniquely to advection.

Several limitations follow directly from the modelling design. The implementation is two-dimensional and depth-averaged; vertical boundary-layer structure is unresolved. The diffusivity is spatially uniform, while the reference and forcing fields are created by interpolation from 48 point locations. The forcing coefficients are effective calibration weights and do not provide a closed surface-energy budget. Finally, both one-step and recursive experiments use prescribed reference-based boundary values, and the recursive experiment also uses known future ERA5-derived forcing.

These limitations define a clear development path. Explicit horizontal advection should be incorporated and tested against the present baseline; spatially varying transport parameters can be informed by land-surface and stability indicators; irregular-domain finite-element formulations can better represent the UAE coastline; and fully prognostic experiments should replace future forcing and boundary values with predicted quantities. Uncertainty quantification and physics-informed machine-learning formulations are natural subsequent extensions once the additional physical processes are introduced and independently validated.

7 Conclusions

This study developed a reduced-order physics-based framework for regional daily near-surface temperature reconstruction and heatwave analysis in an arid environment. The UAE implementation combines a diffusion–forcing PDE with ERA5-derived radiation, sensible-heat and humidity predictors, chronological calibration and a training-only location-specific heatwave definition. Over the held-out test period, one-step reconstruction achieved RMSE = 1.18°C, MAE = 0.83°C and $R^2 = 0.956$, while duration-based heatwave detection achieved F1 = 0.843 and accuracy = 94.2%.

The forcing-only comparison demonstrates that diffusion provides only a marginal incremental benefit over one day, whereas recursive integration shows that its contribution becomes more evident over longer horizons. At the same time, recursive error and warm bias increase with horizon, with $R^2 = 0.761$ and RMSE $= 2.76$°C at 30 days under prescribed forcing and reference-based boundary conditions. These results quantify both the capability and the structural limitations of the reduced formulation.

The framework should therefore be interpreted as a transparent conditional reconstruction model and methodological baseline rather than a replacement for comprehensive atmospheric forecasting systems. Its principal value is that it links measurable environmental forcing to a mathematically explicit heat-transport equation while making the consequences of model reduction directly testable. Future work will incorporate explicit advection, spatially varying transport parameters, irregular-domain discretisation, prognostic forcing and boundary conditions, uncertainty quantification and hybrid physics-informed learning.

Statements and Declarations

Funding

This work was supported by internal research funding from Emirates Aviation University through the Heatwave Project. The funding was provided internally and no grant number was assigned.

Competing Interests

The authors have no relevant financial or non-financial interests to disclose.

Author Contributions

Author Contributions

A.D. conceived the study, developed the overall research framework and methodology, supervised the work, contributed to the mathematical modelling and interpretation of the results, and led the preparation and revision of the manuscript. M.A.H. contributed substantially to methodological development, data preparation, computational implementation, numerical experiments, analysis, visualisation and manuscript preparation. Y.T.T. contributed substantially to methodological development, validation, analysis and interpretation, and critical revision of the manuscript. H.A.A. contributed to project supervision, project administration, funding acquisition and critical review. A.K. contributed to interpretation of the results and critical review. Z.M. contributed to methodological discussion, interpretation of the findings and critical revision of the manuscript. M.F. contributed to methodological discussion, interpretation of the results, and critical review of the manuscript. All authors reviewed and approved the final manuscript.

Data Availability

The processed data supporting the findings of this study are available from the corresponding author upon reasonable request. The underlying meteorological variables were derived from ERA5 reanalysis data.

References

Arbuthnott, K.G., Hajat, S.: The health effects of hotter summers and heat waves in the population of the united kingdom: a review of the evidence. Environmental Health **16**(Suppl 1), 119 (2017) https://doi.org/10.1186/s12940-017-0322-5

Brimicombe, C., Porter, J.J., Di Napoli, C., Pappenberger, F., Cornforth, R., Petty, C., Cloke, H.L.: Heatwaves: An invisible risk in uk policy and research. Environmental Science & Policy **116**, 1–7 (2021) https://doi.org/10.1016/j.envsci.2020.10.021

Buscail, C., Upegui, E., Viel, J.-F.: Mapping heatwave health risk at the community level for public health action. International Journal of Health Geographics **11**, 38 (2012) https://doi.org/10.1186/1476-072X-11-38

Campbell, S., Remenyi, T.A., White, C.J., Johnston, F.H.: Heatwave and health impact research: A global review. Health & Place **53**, 210–218 (2018) https://doi.org/10.1016/j.healthplace.2018.08.017

Gasparrini, A., Armstrong, B.: The impact of heat waves on mortality. Epidemiology **22**(1), 68–73 (2011) https://doi.org/10.1097/EDE.0b013e3181fdcd99

Guo, Y., Gasparrini, A., Li, S., Sera, F., Vicedo-Cabrera, A.M., *et al.*: Quantifying excess deaths related to heatwaves under climate change scenarios: A multicountry time series modelling study. PLoS Medicine **15**(7), 1002629 (2018) https://doi.org/10.1371/journal.pmed.1002629

Imran, H.M., Kala, J., Ng, A.W.M., Muthukumaran, S.: Impacts of future urban expansion on urban heat island effects during heatwave events in the city of melbourne in southeast australia. Quarterly Journal of the Royal Meteorological Society **145**(723), 2586–2602 (2019) https://doi.org/10.1002/qj.3580

Karpatne, A., Atluri, G., Faghmous, J.H., Steinbach, M., Banerjee, A., Ganguly, A., Shekhar, S., Samatova, N., Kumar, V.: Theory-guided data science: A new paradigm for scientific discovery from data. IEEE Transactions on Knowledge and Data Engineering **29**(10), 2318–2331 (2017) https://doi.org/10.1109/TKDE.2017.2720168

Kovats, R.S., Ebi, K.L.: Heatwaves and public health in europe. European Journal of Public Health **16**(6), 592–599 (2006) https://doi.org/10.1093/eurpub/ckl049

LeCun, Y., Bengio, Y., Hinton, G.: Deep learning. Nature **521**, 436–444 (2015) https:

//doi.org/10.1038/nature14539

Lhotka, O., Kyselý, J., Farda, A.: Climate change scenarios of heat waves in central europe and their uncertainties. Theoretical and Applied Climatology **131**(3–4), 1043–1054 (2018) https://doi.org/10.1007/s00704-016-2031-3

Liu, J., Qi, J., Yin, P., Liu, W., He, C., Gao, Y., Zhou, L., Zhu, Y., Kan, H., Chen, R., *et al.*: Rising cause-specific mortality risk and burden of compound heatwaves amid climate change. Nature Climate Change **14**(11), 1201–1209 (2024) https://doi.org/10.1038/s41558-024-02137-5

Lemonsu, A., Viguié, V., Daniel, M., Masson, V.: Vulnerability to heat waves: Impact of urban expansion scenarios on urban heat island and heat stress in paris (france). Urban Climate **14**, 586–605 (2015) https://doi.org/10.1016/j.uclim.2015.10.007

Michelozzi, P., Donato, F.K., Bargagli, A.M., D'Ippoliti, D., De Sario, M., Marino, C., Schifano, P., Cappai, G., Leone, M., Kirchmayer, U., *et al.*: Surveillance of summer mortality and preparedness to reduce the health impact of heat waves in italy. International Journal of Environmental Research and Public Health **7**(5), 2256–2273 (2010) https://doi.org/10.3390/ijerph7052256

Nairn, J.R., Fawcett, R.G.: Defining heatwaves: Heatwave defined as a heat-impact event servicing all community and business sectors in australia. Technical Report 060, Centre for Australian Weather and Climate Research, Melbourne, Australia (2013). https://www.bom.gov.au/research/publications/cawcrreports/CTR_060.pdf

Perkins, S.E., Alexander, L.V.: On the measurement of heat waves. Journal of Climate **26**(13), 4500–4517 (2013) https://doi.org/10.1175/JCLI-D-12-00383.1

Perkins, S.E.: A review on the scientific understanding of heatwaves—their measurement, driving mechanisms, and changes at the global scale. Atmospheric Research **164–165**, 242–267 (2015) https://doi.org/10.1016/j.atmosres.2015.05.014

Powers, J.G., Klemp, J.B., Skamarock, W.C., Davis, C.A., Dudhia, J., Gill, D.O., Coen, J.L., Gochis, D.J., Ahmadov, R., *et al.*: The weather research and forecasting model: Overview, system efforts, and future directions. Bulletin of the American Meteorological Society **98**(8), 1717–1737 (2017) https://doi.org/10.1175/BAMS-D-15-00308.1

Reichstein, M., Camps-Valls, G., Stevens, B., Jung, M., Denzler, J., Carvalhais, N., Prabhat: Deep learning and process understanding for data-driven earth system science. Nature **566**, 195–204 (2019) https://doi.org/10.1038/s41586-019-0912-1

Robinson, P.J.: On the definition of a heat wave. Journal of Applied Meteorology **40**(4), 762–775 (2001) https://doi.org/10.1175/1520-0450(2001)040⟨0762:OTDOAH⟩2.0.CO;2

Skamarock, W.C., Klemp, J.B., Dudhia, J., Gill, D.O., Liu, Z., Berner, J., Wang, W., Powers, J.G., Duda, M.G., Barker, D.M., Huang, X.-Y.: A description of the advanced research wrf model version 4. Technical Report NCAR/TN-556+STR, National Center for Atmospheric Research (2019). https://doi.org/10.5065/1dfh-6p97

Varela, R., Rodríguez-Díaz, L., deCastro, M.: Persistent heat waves projected for middle east and north africa by the end of the 21st century. PLoS ONE **15**(11), 0242477 (2020) https://doi.org/10.1371/journal.pone.0242477

Vanderplanken, K., Van Den Hazel, P., Marx, M., Shams, A.Z., Guha-Sapir, D., Van Loenhout, J.A.F.: Governing heatwaves in europe: comparing health policy and practices to better understand roles, responsibilities and collaboration. Health Research Policy and Systems **19**, 20 (2021) https://doi.org/10.1186/s12961-020-00645-2

Zuo, J., Pullen, S., Palmer, J., Bennetts, H., Chileshe, N., Ma, T.: Impacts of heat waves and corresponding measures: a review. Journal of Cleaner Production **92**, 1–12 (2015) https://doi.org/10.1016/j.jclepro.2014.12.078